DRAFT: Probing for high momentum protons in ^{4}He via the $^4He(e,e'p)X$ reaction

S. Iqbal,[1] F. Benmokhtar,[2,*] M. Ivanov,[3] N. See,[1] K. Aniol,[1,†] D. W. Higinbotham,[4] C. Boyd,[2] S. Gilad,[5] A. Saha,[4,‡] J.M. Udias,[6] J. S. Goodwill,[2] D. Finton,[2] Z. Ye,[7] P. Solvignon,[4,‡] P. Aguilera,[8] Z. Ahmed,[9] H. Albataineh,[10] K. Allada,[4] B. Anderson,[11] D. Anez,[12] J. Annand,[13] J. Arrington,[7] T. Averett,[14] H. Baghdasaryan,[15] X. Bai,[16] A. Beck,[17] S. Beck,[17] V. Bellini,[18] A. Camsonne,[4] C. Chen,[19] J.-P. Chen,[4] K. Chirapatpimol,[15] E. Cisbani,[20] M. M. Dalton,[15,4] A. Daniel,[21] D. Day,[15] W. Deconinck,[5] M. Defurne,[22] D. Flay,[23] N. Fomin,[24] M. Friend,[25] S. Frullani,[20] E. Fuchey,[23] F. Garibaldi,[20] D. Gaskell,[4] R. Gilman,[26] S. Glamazdin,[27] C. Gu,[15] P. Guèye,[19] C. Hanretty,[15] J.-O. Hansen,[4] M. Hashemi Shabestari,[15] O. Hen,[28] M. Huang,[29] G. Jin,[15] N. Kalantarians,[15] H. Kang,[30] A. Kelleher,[5] I. Korover,[28] J. LeRose,[4] J. Leckey,[31] R. Lindgren,[15] E. Long,[11] J. Mammei,[32] D. J. Margaziotis,[1] P. Markowitz,[33] D. Meekins,[4] Z. Meziani,[23] R. Michaels,[4] M. Mihovilovic,[34] N. Muangma,[5] C. Munoz Camacho,[35] B. Norum,[15] Nuruzzaman,[36] K. Pan,[5] S. Phillips,[37] E. Piasetzky,[28] I. Pomerantz,[28] M. Posik,[23] V. Punjabi,[38] X. Qian,[29] Y. Qiang,[4] X. Qiu,[39] P. E. Reimer,[7] A. Rakhman,[9] S. Riordan,[15,40] G. Ron,[41] O. Rondon-Aramayo,[15,4] L. Selvy,[11] A. Shahinyan,[42] R. Shneor,[28] S. Sirca,[43,34] K. Slifer,[37] N. Sparveris,[23] R. Subedi,[15] V. Sulkosky,[5] D. Wang,[15] J. W. Watson,[11] L. B. Weinstein,[10] B. Wojtsekhowski,[4] S. A. Wood,[4] I. Yaron,[28] X. Zhan,[7] J. Zhang,[4] Y. W. Zhang,[26] B. Zhao,[14] X. Zheng,[15] P. Zhu,[44] and R. Zielinski[37]

(The Jefferson Lab Hall A Collaboration)

[1] *California State University, Los Angeles, Los Angeles, CA 90032*
[2] *Duquesne University, Pittsburgh, PA 15282*
[3] *Bulgarian Academy of Sciences, Bulgaria*
[4] *Thomas Jefferson National Accelerator Facility, Newport News, VA 23606*
[5] *Massachusetts Institute of Technology, Cambridge, MA 02139*
[6] *Computense University de Madrid, Spain*
[7] *Physics Division, Argonne National Laboratory, Lemont, IL 60439*
[8] *Institut de Physique Nucléaire (UMR 8608), CNRS/IN2P3 - Université Paris-Sud, F-91406 Orsay Cedex, France*
[9] *Syracuse University, Syracuse, NY 13244*
[10] *Old Dominion University, Norfolk, VA 23529*
[11] *Kent State University, Kent, OH 44242*
[12] *Saint Mary's University, Halifax, Nova Scotia, Canada*
[13] *University of Glasgow, Glasgow G12 8QQ, Scotland, United Kingdom*
[14] *College of William and Mary, Williamsburg, VA 23187*
[15] *University of Virginia, Charlottesville, VA 22904*
[16] *China Institute of Atomic Energy, Beijing, China*
[17] *Nuclear Research Center Negev, Beer-Sheva, Israel*
[18] *Universita di Catania, Catania, Italy*
[19] *Hampton University, Hampton, VA 23668*
[20] *INFN, Sezione Sanità and Istituto Superiore di Sanità, 00161 Rome, Italy*
[21] *Ohio University, Athens, OH 45701*
[22] *CEA Saclay, F-91191 Gif-sur-Yvette, France*
[23] *Temple University, Philadelphia, PA 19122*
[24] *University of Tennessee, Knoxville, TN 37996*
[25] *Carnegie Mellon University, Pittsburgh, PA 15213*
[26] *Rutgers, The State University of New Jersey, Piscataway, NJ 08855*
[27] *Kharkov Institute of Physics and Technology, Kharkov 61108, Ukraine*
[28] *Tel Aviv University, Tel Aviv 69978, Israel*
[29] *Duke University, Durham, NC 27708*
[30] *Seoul National University, Seoul, Korea*
[31] *Indiana University, Bloomington, IN 47405*
[32] *Virginia Polytechnic Inst. and State Univ., Blacksburg, VA 24061*
[33] *Florida International University, Miami, FL 33199*
[34] *Jozef Stefan Institute, Ljubljana, Slovenia*
[35] *Université Blaise Pascal/IN2P3, F-63177 Aubière, France*
[36] *Mississippi State University, Mississippi State, MS 39762*
[37] *University of New Hampshire, Durham, NH 03824*
[38] *Norfolk State University, Norfolk, VA 23504*
[39] *Lanzhou University, Lanzhou, China*
[40] *University of Massachusetts, Amherst, MA 01006*
[41] *Racah Institute of Physics, Hebrew University of Jerusalem, Jerusalem, Israel*
[42] *Yerevan Physics Institute, Yerevan 375036, Armenia*

[43] *Faculty of Mathematics and Physics, University of Ljubljana, Ljubljana, Slovenia*
[44] *University of Science and Technology, Hefei, China*

(Dated: April 29, 2019)

Experimental cross sections for the $^4He(e,e'p)X$ reaction up to a missing momentum of 0.632 GeV/c at $x_B = 1.24$ and Q^2=2(GeV/c)^2 are reported. The data are compared to Relativistic Distorted Wave Impulse Approximation(RDWIA) calculations for $^4He(e,e'p)^3H$ channel. Significantly more events in the triton mass region are measured for p_m>0.45 GeV/c than are predicted by the theoretical model, suggesting that the effects of initial-state multi-nucleon correlations are stronger than expected by the RDWIA model.

PACS numbers: 13.60.Hb, 25.10.+s, 25.30.Fj

I. INTRODUCTION

Nucleon momentum distributions in atomic nuclei are known to be governed by an average nuclear potential plus additional nucleon-nucleon multi body interactions. Momentum distributions below the Fermi momentum essentially reflect the size of the "box" in which the nucleons are contained. One way to model this distribution is in the simplest limit of a cluster model where a given nucleon interacts with the average potential of the other nucleons. For momenta greater than the Fermi momentum the cluster models of nuclear structure provide enhanced strength in the momentum distribution by allowing nucleon-nucleon spatial distributions to become shorter than the average nucleon-nucleon spacing. Experimental access to proton momentum distributions is possible through the missing momentum p_m and the missing energy E_m in the $A(e,e'p)X$ reaction. Where $\vec{p}_X = \vec{p}_e - \vec{p}_{e'} - \vec{p}_p$, $p_m = |\vec{p}_X|$, is the momentum of the residual nucleus [1]. The missing energy, E_m, of the reaction is the excitation energy of the system; it is the difference between the electron transferred energy (ω=$E_e - E_{e'}$) and the kinetic energies of the knocked out proton and the residual system, T_p and T_X, respectively: $E_m = \omega - T_p - T_X$.

Interpretation of cross sections $\sigma(p_m)$ to deduce nucleon momentum distributions requires the inclusion of final state interactions in the outgoing ($e'pX$) system.

Microscopic nuclear structure calculations based on realistic two and three body nucleon-nucleon calculations are available for low mass nuclei [2]. In the case of ^{4}He proton momentum distributions have been calculated for proton-triton(pt) and deuteron-deuteron(dd) clusters. Recent measurements of proton-nucleon coincidences in the $^4He(e,e'pN)$ reaction [3–6] have shown strong correlations of back to back emission of nucleon pairs for large missing momentum p_m>400 MeV/c. Moreover, the increasing pair ratio $\frac{\#pp}{\#pn}$ as a function of p_m>400 MeV/c is interpreted as a sign that the nucleon-nucleon interaction switches from the tensor interaction to the strong repulsive short range interaction. Besides nucleon-nucleon correlations the experiment also obtained data on the proton-triton (pt) final hadronic state.

This paper provides experimental differential cross sections based on the $^4He(e,e'p)3N$ reaction over a range of momenta, 25<p_m<632 MeV/c, where $3N = {}^3H$ and X. These experimental results are compared to state-of-the-art relativistic calculations.

These measurements ran in parallel with the triple-coincidence short-range correlation experiment described in Ref. [3].

II. EXPERIMENTAL SETUP

A. Spectrometer settings

Experiments E07006 [3] and E08009 [7] at the Thomas Jefferson National Accelerator Facility in experimental Hall A [8], ran in February, March and April of 2011. Data for kinematic settings of 0.153 and 0.353 GeV/c missing momentum were obtained using electron beam currents between 47μA to 60μA, for E08009. In addition to these kinematic settings the Short Range Correlation(SRC) [3] experiment also obtained data at kinematic settings out to 0.632 GeV/c missing momentum including the multi-body break up channel p+3N. These higher missing momenta data were collected using 4 to 5 μA electron beam currents but sufficient accumulated charge was measured to be able to extract cross sections beyond the original goal set for E08009. Moreover, the acceptances of the Hall A spectrometers allowed for cross sections to be determined across a larger missing momentum range than the central value kinematic settings would suggest.

The electron spectrometer was fixed in angle and central momentum while the proton spectrometer's angles and central momenta were changed.

Electron arm's kinematic settings for the experiment are as follows: incident beam energy 4.4506 GeV, electron spectrometer angle 20.3° electron spectrometer momentum 3.602 GeV/c, four momentum transfer $Q^2 = 2.0$ (GeV/c)^2 and Bjorken x_b=1.24, 3 momentum transfer of

* Contact person benmokhtarf@duq.edu
† Contact person kaniol@calstatela.edu
‡ deceased

Central p_m	θ_p	θ_{pq}	Central momentum
GeV/c	degrees	degrees	GeV/c
0.153	47.0	-2.4	1.500
0.353	38.5	-10.9	1.449
0.466	33.5	-15.9	1.383
0.632	29.0	-20.4	1.308

TABLE I. Proton spectrometer settings

1.647 GeV/c at an angle $\theta_q = 49.4^\circ$ with respect to the incident electron momentum. The proton arm settings are in table I.

B. Cryogenic target

The cryogenic target was gas ^{4}He contained in an aluminum can of length 20 cm. The nominal temperature of the gas was 20° K at 199 psia. ^{4}He enters and exits at the upstream end of the target.There is no outlet for the fluid at the downstream end of the can. A determination of target density along the beam path was done by comparing the normalized yield of scattered electrons at $47\mu A$ and $60\mu A$ beam currents to the yield at $4\mu A$. Since the electron spectrometer was held at a fixed momentum and angle the electron spectrometer served as a density monitor. For this target at a beam current of $4\mu A$ a computational fluid dynamics (CFD) calculation [9] predicts an average density drop of 2.3% from strictly thermodynamic parameters. A comparison of the measured yield at $4\mu A$ to the CFD calculation gives an uncertainty in the target density dependence along the beam of 1.1%. More detail for the treatment of the target density used in the data analysis is available in [7]. Across the $\pm$ 8cm effective target length and for the different beam currents, the target densities are summerized in table II.

III. DATA ANALYSIS

For this experiment, event triggers were performed by coincident signals from scintillator arrays. Particle tracks were reconstructed using the high resolution spectrometer's vertical drift chambers. The small π^- background in the electron arm was rejected using a CO_2 gas Cherenkov detector. In the proton spectrometer, coincident π^+, and other positively charged nuclei like ^{2}H, and ^{3}H were separated from the protons using the time difference between particles detected in the two spectrometers. Most of the accidental coincident events were rejected by cuts on the difference between interaction points in the target along the beam as reconstructed by the two spectrometers. The remaining accidental background was subtracted using the coincidence timing between the spectrometers. Fig. 1 shows a coincidence time of flight for the 353 MeV/c kinematics. The number of real coincidence events in a 20 ns time window around the peak were obtained by subtracting the accidentals under the peak considering a flat background under the whole spectrum. 1.

For the determination of the cross section the following cuts are applied to the data for both electron and proton spectrometers: horizontal angle ± 0.04 radians, vertical angle ± 0.03 radians, vertex position ± 8 cm and the deviation from central momentum $\pm 4.5\%$. The full data set after accidental and background subtraction is presented in figure 2.

The average cross section for the $^4He(e,e'p)X$ reaction per missing momentum bin was extracted for the triton region and it is given by:

$$< \sigma(p_m) >= \frac{n(p_m) * RSC}{\Delta\Omega_e \Delta\Omega_p \Delta E_e N_e N_{tgt} * EFF}. \quad (1)$$

- $n(p_m)$ is the net counts in the triton region between missing energies of 0.017 GeV to 0.022 GeV, after randoms and background subtraction. The three nucleon region, 3N, lies between 0.017 GeV and 0.029 GeV in the missing energy spectrum. Background subtraction in the triton region was done using either a simple constant background or a sloped straight line background below 0.029 GeV.
- RSC is the radiative and straggling correction factor, more details on this correction are given in section III B.
- $\Delta\Omega_e$ and $\Delta\Omega_p$ are the geometrical solid angles of the spectrometer apertures.
- ΔE_e is the size of the electron's momentum bin in coincidence with protons.There is an uncertainty in ΔE_e of 10% which is included in the error bars of the cross sections.
- $N_e = Q/e$, the number of electrons that passed through the target, where e is the charge on an electron and Q is the total charge.
- $N_{tgt} = \rho(I) * z_{tgt}$ is the number of nuclei per cm^2 in the beam. I is the beam current, $\rho(I)$ is the number of nuclei per cm^3 and z_{tgt} is the effective target length. Target densities along the $\pm$ 8cm effective target length for different beam currents are presented in table II.
- EFF is the efficiency factor and it accounts for: a missing momentum acceptance factor (explained in section III A), data acquisition live time, electronics live time, wire chamber and tracking efficiencies. The live time of the trigger acquisition system, $LTdaq$, was 0.916 ± 0.01, and 0.95 ± 0.01 for the 153 MeV/c and 353 MeV/c kinematics, respectively. For the higher missing momentum settings, $LTdaq$ was larger than 0.99. The remaining efficiencies are displayed in table III.

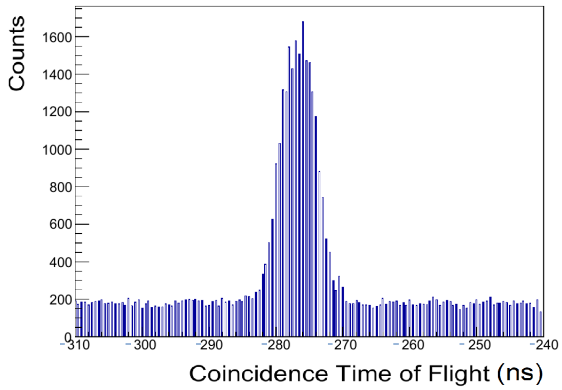

FIG. 1. Coincidence time of flight spectrum for the 353 MeV/c setting.

Beam current (μA)	Target density $nuclei/cm^2$
4.014	$7.84 \pm 0.087 \times 10^{22}$
45.46	$6.732 \pm 0.077 \times 10^{22}$
60.71	$5.662 \pm 0.065 \times 10^{22}$

TABLE II. Target density dependence on beam heating as a function of beam current.

Efficiency	value	Uncertainty (%)
Electronic live time	1	0
Trigger efficiency	0.97	1
Wire chamber efficiency	0.995	0.1
Tracking efficiency	0.9895	0.75

TABLE III. General uncertainties

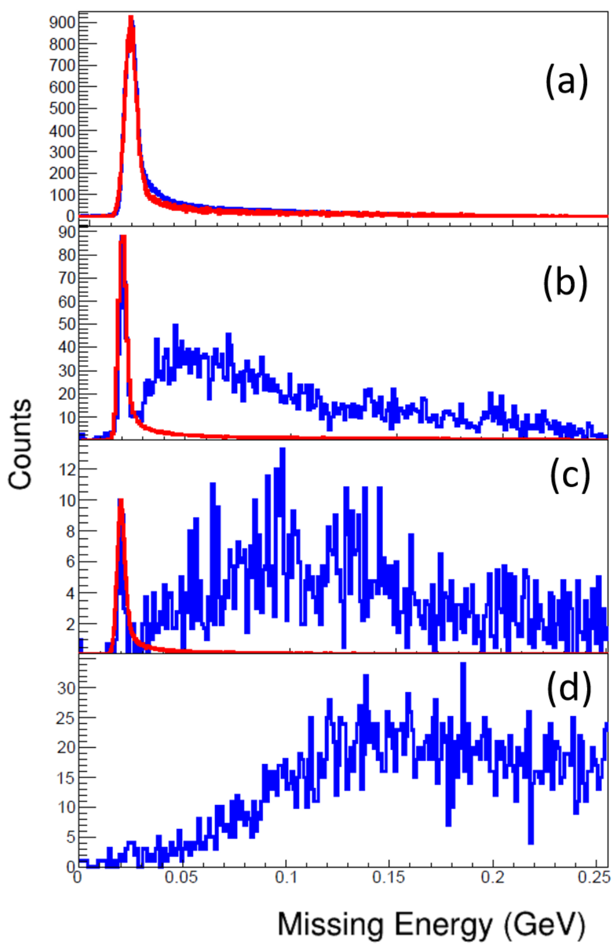

FIG. 2. Missing Energy spectra for all the kinematical settings. Data are in blue and the simulated two body breakup channel is in red. From top to Bottom: (a) p_m = 153 MeV/c, (b) p_m =353 MeV/c, (c) p_m=466 MeV/c and (d) p_m=632 MeV/c

Data analysis is aided by the Monte Carlo simulation(GEANT 3.2 [10]) of the transport of the incident electron, scattered electron and proton through the target cell into the spectrometer apertures assuming a p + triton final hadronic state. The identification of the p + triton final state is possible by calculating the missing energy in the scattered electron + p state. A peak in the missing energy spectrum corresponding to the triton ground state mass identifies the $^4He(e,e'p)^3H$ reaction, where m$_X$ = triton mass, as seen in figure 2.

A. Missing momentum acceptance efficiency

The wide momentum acceptance of the spectrometers allows for a broad missing momentum acceptance. In the simulation a vertex point in the gas target is chosen which gives the incoming electron's momentum at interaction point. Then hit points within the apertures of the spectrometers for the outgoing electron and proton are randomly selected. Each point within the spectrometers' apertures has an equal probability of being selected. This allows for the vertex angles of the electron and proton to be determined. An energy for the outgoing electron is chosen within the momentum acceptance of the electron spectrometer. From the incident electron's momentum, the scattered electron's momentum and the angles for the ejected proton three body kinematics for the $^4He(e,e'p)^3H$ reaction allows for the proton's vertex momentum to be determined. The electron and proton are followed from the vertex to the final hit points in the spectrometers' apertures. Thus complete information about the location and momenta at the vertex and the spectrometers' apertures is known.

The three body kinematical and geometrical limitations for particles arriving at the hit points within the apertures are calculated by GEANT and thus allows the missing momentum, $\vec{p_m} = \vec{p_1} - \vec{p_2} - \vec{p_p}$ to be calculated. In the analysis we bin $|\vec{p_m}|$ into 50 MeV/c bins. We define the missing momentum acceptance factor, $f(p_m)$, for a bin of missing momentum centered around p_m as

$$f(p_m) = \frac{n(p_m)}{\sum n(p_m)}. \tag{2}$$

where $n(p_m)$ is the number of triton events in the missing momentum bin centered on p_m and $\sum n(p_m)$ is the total number of triton events over all missing momenta for the particular proton kinematic setting. The same Gaussian broadening used for the simulation fit in figure 2 (b) is used to generate the values of p_m needed to calculate $f(p_m)$.

Experimental cross sections are given in table IV.

B. Peak broadening effects

Straggling and external bremsstrahlung obtained from the GEANT simulation produce a broadening and a characteristic tail on the missing energy spectrum. In practice the long target introduces additional broadening beyond the intrinsic point source resolution of the spectrometers. The additional broadening is included in the simulation by a Gaussian broadening of the momenta at the apertures This additional broadening typically is a factor of three to four bigger than the resolution for the point source peak. The amount of Gaussian smearing needed is determined by the best fit of a strong missing energy data peak such as at the lowest missing momentum. An example of the fit is seen in figure 2(b).

Corrections to the cross section due to the tail on the missing energy spectrum are determined by comparing the number of events in a 5 MeV window centered on the triton peak to the total number of events in the simulation.

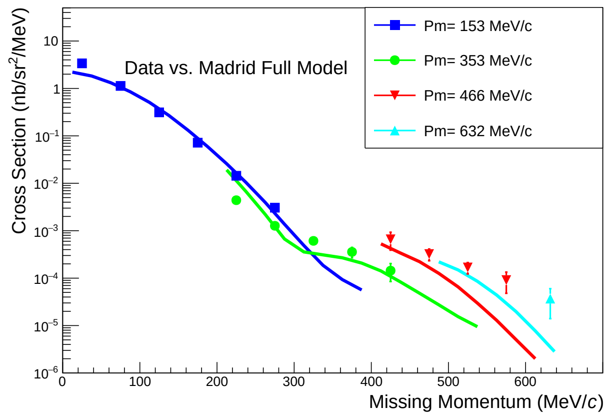

FIG. 3. E08009 Data compared to Madrid full theoretical calculations. Blue squares are for the 153 MeV/c setting, green circles are for the 353 MeV/c setting, red inverted triangles are for the 466 MeV/c setting and cyan triangles are for the 632 MeV/c setting. Theoretical calculation follow the same color code as the data for each momentum setting.

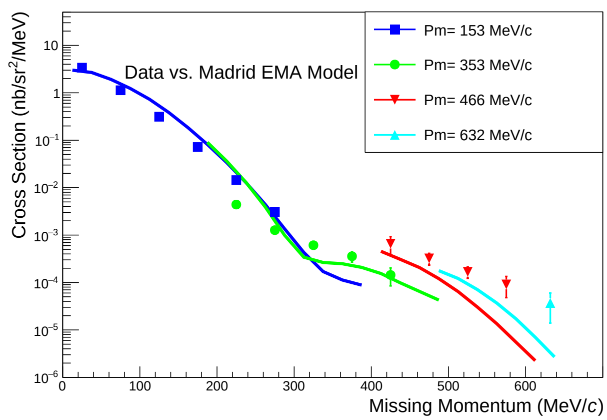

FIG. 4. E08009 Data compared to Madrid EMA theoretical calculations. Blue squares are for the 153 MeV/c setting, green circles are for the 353 MeV/c setting, red inverted triangles are for the 466 MeV/c setting and cyan triangles are for the 632 MeV/c setting. Theoretical calculation follow the same color code as the data for each momentum setting.

IV. RESULTS

A. Comparison of data to theoretical predictions

Experimental differential cross sections are compared to relativistic distorted wave impulse approximation calculations of the Madrid theory group [11–14]. The ^{4}He ground state is described by a relativistic solution of the Dirac equation phenomenologically adjusted to fit the observed radius and binding energy of ^{4}He. These calculations were first introduced in [15].

Vertex values of the incident electron's momentum at various positions within the target and the momenta of the scattered electron and ejected proton were provided to the Madrid theory group for calculation of the cross section at each event vertex in the GEANT simulation. The GEANT simulation also contains the detected electron and proton momenta at the spectrometers' apertures. In this way the vertex cross section can be associated with the missing momentum at the apertures.

Theoretical cross sections integrated over the experimental acceptances for the full Madrid treatment and using the effective momentum approximation, EMA, treatment are presented in tables V and VI. Plots of the data for the two theoretical treatments are shown in figures 3 and 4.

Data and calculations show the same missing momenta dependence for the measured or calculated cross section as a function of kinematic setting. Even though the same magnitude of p_m is reached for different proton angles the cross section does not simply factor as a function of p_m. Good agreements between the Madrid calculation and the data extend to about 420 MeV/c in missing momentum. It can be also noticed that both data and theory exhibit an inflection in the slope of the cross section between 300 and 400 MeV/c. In recent calculations on light nuclei [2], an inflection in the proton momentum distributions was predicted in the momentum range between 1 and 3 fm^{-1}. For ^{4}He, this inflection appears to be due to the triton+proton cluster distribution exhibiting a deep minimum in the proton momentum distribution. When added to the deuteron deuteron cluster distribution, the inflection appears below and close to 2 fm^{-1} in the total proton density distribution, which is in agreement with the one we see in these data.

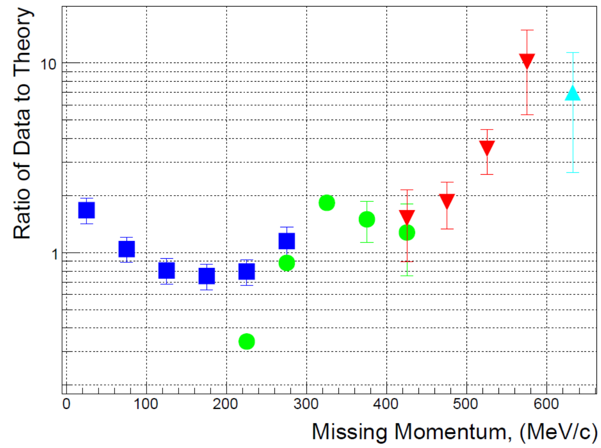

FIG. 5. Ratio of the experimental cross section to the theoretical Madrid full (pt) cross section versus missing momentum. Squares are for the 153 MeV/c setting, circles are for 353 MeV/c setting, inverted triangles are for the 466 MeV/c setting and triangles are for the 632 MeV/c setting.

V. DISCUSSION

For this experiment, the three momenta of the outgoing proton and scattered electron in the $^4He(e,e'p)X$ reaction are measured. Using the known momentum of the initial state we deduce the missing momentum of the residual hadronic state X. The theoretical analysis of the data here is limited to a specific exit channel, $X =$ ^{3}H. However, considering the theoretical cluster contributions to the proton momenta [2] in ^{4}He, the contribution of the pt cluster to the proton momentum distribution is expected to be negligible above about p_m =250 MeV/c.

The ratio of experimental cross section to the Madrid full predictions; in logarithmic scale, is shown in figure 5 for the four proton spectrometer central momentum settings. The blue squares; at the lowest missing momentum setting, hover around a ratio of 1, showing good agreement between data and predictions. The green dots are for the 0.353 GeV/c setting and we see a distinctive pattern for these data. The ratio at 0.225 GeV/c is 0.34, substantially different from the model prediction. This behavior cannot be traced to a statistical fluctuation because as we see in figure 2 (b), there is a substantial peak at the triton missing energy location. The cross section decreases by a factor of 12 between 0.225 and 0.325 GeV/c and over the full range in missing momentum for this proton angle setting the cross section falls by a factor of 30. This fluctuation of the data to theory ratio suggests that some significant physics is not adequately included in the theoretical model for this range of missing momentum with these spectrometer settings. For the data at the 0.466 and 0.632 GeV/c settings the ratio again shows a smooth missing momentum dependence.

However, the overall dependence of the cross section by the Madrid full model in figure 3 is qualitatively described.

From [2], the high proton momentum is attributed to the repulsive nucleon-nucleon core. Fig. 2 shows a broad peak in the missing energy spectrum which shifts in position kinematically with the photon being absorbed on a correlated pair of nucleons. This feature has been previously seen in $^3He(e,e'p)pn$ measurements in Ref. [16] and [17] and in $^4He(e.e'p)X$ continuum channel in Ref.[18].

The measurements of [3] are consistent with the NN short range force becoming repulsive. However, it is counter intuitive and in disagreement with theoretical expectations [2] that tritons should be ejected from ^{4}He along with protons emerging from short range encounters.

The fact that we observe events in the triton region up to 632 MeV/c involves processes beyond the impulse approximation. Final state interactions of the outgoing proton may take a proton knocked out of a pt cluster initially at a low value of p_p to appear as if its momentum at the vertex was p_m. This is accounted for to some extent by the optical model potential treatment of the final pt unbound state. We see good agreement between the theory and data in figure 3 up to about p_m=420 MeV/c.

Beyond about 450 MeV/c in p_m substantially more triton region events are measured than what the Madrid full theory predicts. In this case three nucleons emitted at high p_m may be a signature of other reactions allowing the three nucleon cluster to emerge as a bound or quasi bound state. Since the kinematics for the electron were chosen for x_b =1.24, protons in more intimate interactions with neighbors than quasi-elastic conditions($x_b \approx 1$) may favor other reactions leading to three nucleon clusters exiting in the missing energy region near the triton.

Portions of the missing energy spectrum in the triton energy range are shown in figures 6. We see a change in the distribution of events as a function of missing momentum going from 153 MeV/c to 575 MeV/c. At low missing momenta the triton peak is centered at the expected value of 19.8 MeV. At higher missing momenta, the event are higher in missing energy by few MeVs. From left to right, the three arrows in each figure point to the expected locations of the thresholds of the hadronic states X=(t), X=(n,d) and X=(p,n,n), respectively.

An interesting question is the impact of three-nucleon forces, V_{ijk}, at high p_m. V_{ijk} are known to increase the binding energy of nuclei [19] so they would be natural actors in the formation of bound tritons or closely bound three nucleon groups among the outgoing hadronic channels, X, at high missing momentum. The principal sources of data to help refine models of possible three-nucleon interactions are binding energies of ground and excited states of $A < 8$ nuclei and point proton charge distributions [19]. However, these data are not extensive enough to select unambiguously a particular set of parameters or models for V_{ijk} and other observables are needed as discussed in [19] [20].

More extensive and detailed data in the three nucleon triton mass region and the existence of microscopic calculations for these nuclei opens the possibility of exploiting the shapes of the missing energy spectra in $A(e, e'p)X$ reactions as additional observables for developing models of three-nucleon interactions.

ACKNOWLEDGMENTS

Special thanks to Silviu Covrig for providing the CFD calculations as a possibility to understanding the target vertex spectra for the SRC Target. The research presented in this paper is partially supported by the U.S. National Science Foundation grants PHY 09-69380 and PHY 12-08056. This work was supported by the U.S. Department of Energy contract DE-AC05-06OR23177 under which Jefferson Science Associates operates the Thomas Jefferson National Accelerator Facility.

VI. APPENDIX

Experimental differential cross sections for $^4He(e, e'p)X$; in $nb/sr^2/MeV$, are summarized in table IV for the four different spectrometer settings. The analysis was done on 50 MeV/c wide bins on missing momentum, p_m. Errors are both statistics and systematics added in quadrature. The systematic uncertainty of 10% was included in the cross sections due to defining the size of the energy window, dE_e, on the electron spectrum.

Tables VI and V summarize the Madrid EMA and full calculations respectively in the momentum range from 12.5 to 637.5 MeV/c.

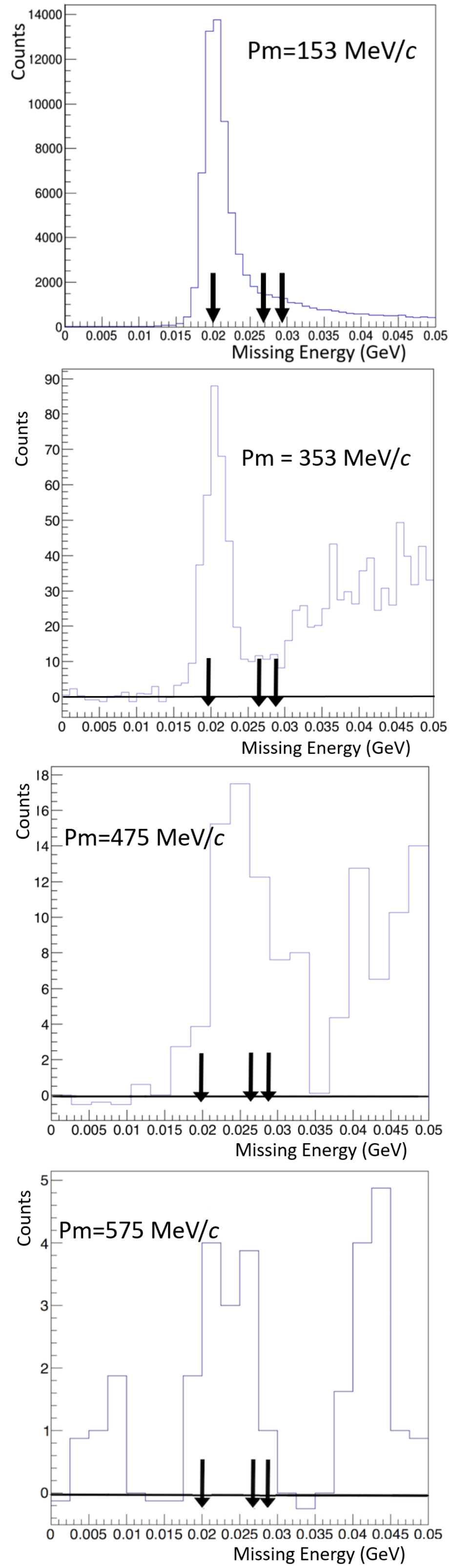

FIG. 6. From top to bottom: Missing energy region up to 50 MeV of excitation in $^4He(e, e'p)X$ for p_m=153, 352, 475 and 575 MeV/c, respectively. The three arrows point to the expected locations of the thresholds of the hadronic states X=(t), X=(n,d) and X=(p,n,n).

p_m (MeV/c)	153 $\theta_p = 47^\circ$	353 $\theta_p = 38.5^\circ$	466 $\theta_p = 33.5^\circ$	632 $\theta_p = 29^\circ$
25	(3.38 ± 0.52)			
75	(1.13 ± 0.17)			
125	$(3.13 \pm 0.48) \times 10^{-1}$			
175	$(7.18 \pm 1.1) \times 10^{-2}$			
225	$(1.44 \pm 0.22) \times 10^{-2}$	$(4.40 \pm 0.14) \times 10^{-3}$		
275	$(3.06 \pm 0.57) \times 10^{-3}$	$(1.27 \pm 0.03) \times 10^{-3}$		
325		$(6.11 \pm 0.14) \times 10^{-4}$		
375		$(3.57 \pm 0.88) \times 10^{-4}$		
425		$(1.44 \pm 0.59) \times 10^{-4}$	$(6.59 \pm 2.7) \times 10^{-4}$	
475			$(3.22 \pm 0.89) \times 10^{-4}$	
525			$(1.68 \pm 0.45) \times 10^{-4}$	
575			$(0.91 \pm 0.43) \times 10^{-4}$	
632				$(3.7 \pm 2.3) \times 10^{-5}$

TABLE IV. Experimental differential cross sections, $\frac{d\sigma^5}{d\Omega_p d\Omega_e dE_e}$, for $^4He(e,e'p)X$; where $X = {}^3H$ or $3N$, from E08009, for different kinematical settings given by the proton spectrometer central angle. Units are $nb/sr^2/MeV$.

[1] J. J. Kelly, Adv. Nucl. Phys. **23**, 75 (1996), [,75(1996)].

[2] R. Wiringa, *et al.*, Phys. Rev. C **89**, 024305 (2014).

[3] I. Korover, *et al.*, Phys. Rev. Lett. **113**, 022501 (2014).

[4] R. Schiavilla, R. B. Wiringa, S. C. Pieper, and J. Carlson, Phys. Rev. Lett. **98**, 132501 (2007), arXiv:nucl-th/0611037 [nucl-th].

[5] M. M. Sargsian, T. V. Abrahamyan, M. I. Strikman, and L. L. Frankfurt, Phys. Rev. **C71**, 044615 (2005), arXiv:nucl-th/0501018 [nucl-th].

[6] M. Alvioli, C. Ciofi degli Atti, and H. Morita, Phys. Rev. Lett. **100**, 162503 (2008).

[7] Sophia Iqbal California State University, Los Angeles 2013, DOE/OR/23177-3086, `https://misportal.jlab.org/ul/publications/view_pub.cfm?pub_id=13189`.

[8] J. Alcorn *et al.*, Nucl. Instrum. Meth. **A522**, 294 (2004).

[9] Silviu Covrig, Computational Fluid Dynamics, private communication (2012).

[10] Instructions for COMGEANT, `https://userweb.jlab.org/~gen/simul/`.

[11] J. M. Udias, *et al.*, Proceedings of the 5$^{\text{th}}$ Workshop on Electromagnetically Induced Two-Hadron Emission, ed. P. Grabmayr, Lund, June $13 - 16, 2013$ arXiv:0109077v1 [nucl=th].

[12] S. P. Malace, *et al.* Phys. Rev. Lett. **106**, 052501 (2011).

[13] R. Álvarez Rodríguez, *et al.*, Few-Body Systems **50**, 359 (2011).

[14] J. M. Udias and J. R. Vignote, Phys. ReV. C **62**, 034302 (2000).

[15] M. Paolone, *et al.*, Phys. ReV. Lett. **105**, 072001 (2010).

[16] F. Benmokhtar, *et al.,* Phys. Rev. L **94** (2005).

[17] C. Marchand, *et al.,* Phys. Rev. L **60** (1988).

[18] J. M. Le-Goff, *et al.,* Phys. Rev. C **50** (1994).

[19] S. C. Pieper, *et al.*, Phys. Rev. C **64**, 014001 (2001).

[20] D. Lonardini, *et al.,* Phys. Rev. C **96**, 024326 (2017).

p_m (MeV/c)	153 $\theta_p = 47^\circ$	353 $\theta_p = 38.5^\circ$	466 $\theta_p = 33.5^\circ$	632 $\theta_p = 29^\circ$
12.5	2.2059			
37.5	1.8287			
62.5	1.3139			
87.5	8.516e-01			
112.5	5.070e-01			
137.5	2.699e-01			
162.5	1.311e-01			
187.5	5.987e-02			
212.5	2.583e-02	1.918e-02		
237.5	1.044e-02	6.724e-03		
262.5	3.951e-03	2.209e-03		
287.5	1.370e-03	6.686e-04		
312.5	4.901e-04	3.578e-04		
337.5	1.858e-04	3.095e-04		
362.5	9.309e-05	2.687e-04		
387.5	5.639e-05	2.077e-04		
412.5		1.419e-04	5.283e-04	
437.5		8.366e-05	3.402e-04	
462.5		4.808e-05	2.225e-04	
487.5		2.739e-05	1.262e-04	2.206e-04
512.5		1.542e-05	6.542e-05	1.491e-04
537.5		9.478e-06	2.980e-05	8.585e-05
562.5			1.289e-05	4.400e-05
587.5			5.077e-06	1.977e-05
612.5			2.008e-06	7.741e-06
637.5			8.357e-07	2.834e-06

TABLE V. Madrid full theoretical cross sections integrated over the experimental acceptances for $^4He(e,e'p)^3H$ for E08009, for different kinematical settings given by the proton spectrometer central angle. Units are $nb/sr^2/MeV$.

p_m (MeV/c)	153 $\theta_p = 47°$	353 $\theta_p = 38.5°$	466 $\theta_p = 33.5°$	632 $\theta_p = 29°$
37.5	2.681			
62.5	1.916			
87.5	1.235			
112.5	7.297e-01			
137.5	3.839e-01			
162.5	1.834e-01			
187.5	8.159e-02	9.031e-02		
212.5	3.382e-02	3.628e-02		
237.5	1.282e-02	1.295e-02		
262.5	4.433e-03	3.933e-03		
287.5	1.362e-03	9.986e-04		
312.5	4.312e-04	3.423e-04		
337.5	1.705e-04	2.643e-04		
362.5	1.130e-04	2.487e-04		
387.5	8.817e-05	2.083e-04		
412.5		1.547e-04	4.550e-04	
437.5		9.853e-05	3.082e-04	
462.5		6.482e-05	2.064e-04	
487.5		4.261e-05	1.206e-04	1.778e-04
512.5			6.435e-05	1.215e-04
537.5			3.036e-05	7.084e-05
562.5			1.360e-05	3.702e-05
587.5			5.527e-06	1.717e-05
612.5			2.251e-06	7.010e-06
637.5			9.483e-07	2.695e-06

TABLE VI. Madrid EMA theoretical cross sections integrated over the experimental acceptances for $^4He(e,e'p)^3H$ for E08009, for different kinematical settings given by the proton spectrometer central angle. Units are $nb/sr^2/MeV$.